Nanoscale

Accepted Manuscript

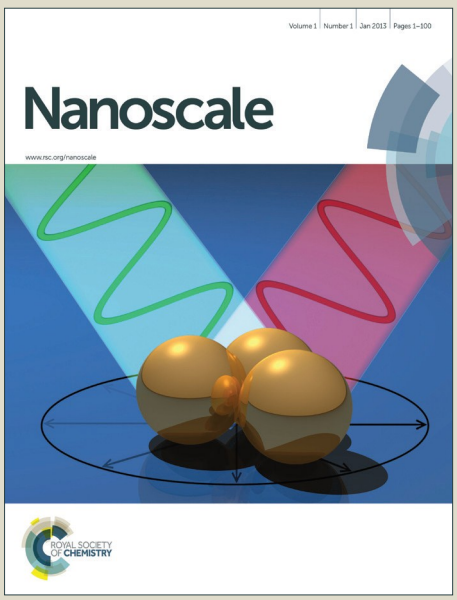

ROYAL SOCIETY OF CHEMISTRY

www.rsc.org/nanoscale

Nanoscale

PAPER

Nanofocusing beyond the near-field diffraction limit via plasmonic Fano resonance

Maowen Song,[a,b,c] Changtao Wang,[a] Zeyu Zhao, [a] Mingbo Pu,[a] Ling Liu,[a] Wei Zhang,[a,c] Honglin Yu,[b] and Xiangang Luo *[a]

The past decade has witnessed a great deal of optical systems designed for exceeding the Abbe's diffraction limi Unfortunately, deep subwavelength spot is obtained at the price of extremely short focal length, which is indeed a nea field diffraction limit that could rarely go beyond in the nanofocusing device. One method to mitigate such problem is t set up a rapid oscillatory electromagnetic field that converges at the prescribed focus. However, abrupt modulation o phase and amplitude within small fraction of a wavelength seems the main obstacles in visible regime, aggravated by and plasmonic features come into function. In this paper, we propose a periodically repeated ring-disk complementary structure to break the near-field diffraction limit via plasmonic Fano resonance, originated from the interference betw the complex hybrid plasmon resonance and the continuum of propagating waves through the silver film. This plasmonic Fano resonance introduces a π phase jump in the adjacent channels and amplitude modulation to achieve radiation electromagnetic interference. As a result, deep subwavelength spots as small as $0.0045\lambda^2$ at 36 nm above the silver fil have been numerically demonstrated. This plate holds promise for nanolithography, subdiffraction imaging and microscopy.

Received 00th January 20xx,
Accepted 00th January 20xx

DOI: 10.1039/x0xx00000x

www.rsc.org/

Introduction

Subdiffraction focusing has attracted a tremendous amount of attention in recent years. The interest is mainly driven by the hope of achieving nanolithography application, near-field data storage and noncontact sensing etc. Unfortunately, it is taken for granted that the smallest focal spot obtained by conventional lens is restricted by the operating wavelength and numerical aperture.[1] Although many nanostructures have been proposed to replace traditional lens, their resolution is still limited owing to the exponential decay of the evanescent wave.[2-4] In order to overcome the far-field diffraction limit, near-field probes such as tapered waveguide apertures and nanoscaled metal/dielectric tips have been designed[5] aiming at capturing the evanescent components before they vanish. However, the ultra short working distance increases the complexity of accurate probe placements in nanolithography techniques, which is indeed a near-field diffraction limit: the spot size is strongly constrained by the incident wavelength and working distance.[6] To relax such crucial tasks for confining the energy at a larger distance, negative refraction based perfect lens has been proposed in 2000.[7] With benefits of negative bending of light and evanescent waves amplification enabled by plasmon response of a metal film, this method produces a subdiffraction imaging/focusing at the other side of the lens which has been numerically and experimentally demonstrated at microwave, infrared, and optical regimes.[8-11]

Inspired by Fresnel plates, the proposal of near-field plates (NFP) provides intriguing opportunities to engineer the phase and amplitude profile of the near-field distribution to produce desired focal pattern.[12] Resulting from manipulation of evanescent waves, these plates are capable of forcing the incident electromagnetic wave to converge to a deep subwavelength spot at some distances away.[12,13] Particularly, a rapid transverse oscillation in the near field has been created and extremely narrow central lobe can be theoretically achieved through the destructive interference between the evanescent components in the source field. This "Radiationless Electromagnetic Interference (REI)" method is based on the ideas of reconstructing the source field at the structure by utilizing the back-propagation calculations from the desired energy distribution at the focal plane. In recent years, different schemes have been experimentally demonstrated at microwave wavelengths[14-16] and numerically extended to visible regimes.[17,18] Nonetheless, complicated structures are usually required for REI focusing systems and the low field intensity at focal plane due to the exponential decay of the field strength precludes its widespread use as lens for general-purpose applications.

[a] State Key Laboratory of Optical Technologies on Nano-Fabrication and Micro-Engineering, Institute of Optics and Electronics, Chinese Academy of Science, P.O. Box 350, Chengdu 610209, China. E-mail: lxg@ioe.ac.cn
[b] Key Laboratory of Optoelectronic Technology and System, Ministry of Education, Chongqing University, Chongqing 400044, China. E-mail: hlyu@cqu.edu.cn
[c] University of Chinese Academy of sciences, Beijing 100049, China.

† Electronic Supplementary Information (ESI) available: The plasmon hybridization modes have been analyzed. The transmittance, reflectance and absorbance have been plotted to have a better understanding of the coupling in a silver nanoring. The dependencies of the intensity enhancement on the total numbers of building blocks have been shown.

One approach to overcome such difficulties lies in combining REI with evanescent field amplification. The excitation of the surface plasmon (SP) gives an opportunity to compensate for the evanescent decay.[19-23] Interestingly, with benefits of unprecedented control of the spectral response[24-33] and ultrahigh quality factor proposed in our previous work,[34] Fano resonance (FR) that occurs from interference between a discrete state and a continuous state has been exploited as a novel REI method to obtain a narrower and brighter focus.[35] What conceptually unites FR and REI is suppressing radiation by destructive interference and local field enhancement which compensates the decay of the evanescent components. Complicated mode matching theory shows that the full-width at half-maximum (FWHM) of the *x* component electric field intensity is about 53 nm with focal length of 32 nm at optical wavelengths. However, such performance is just comparable to typical REI approach or negative refraction lens according to the metric of evanescent wave amplification proposed by Gordon.[36] Furthermore, one-dimensional focusing and a limitation on size placed by nanofabrication technology hamper the popularization of this design.

Despite lots of methods have been proposed, near-field diffraction limit still impedes their transition to real applications. In this paper, we propose an alternative approach to realize subdiffraction focusing by REI with evanescent wave amplification at 633 nm. It is shown that a ring-disk complementary structure possesses plasmonic Fano resonance when the hybrid plasmon response meets a spectrally broad resonance. This coupling leads to abrupt π phase change and amplitude modulated electromagnetic fields exiting the structure, which contribute for a deep subwavelength field confinement ($0.0045\lambda^2$) accompanying obvious field enhancement at the focal plane. With additional advantages of exceeding the metric of evanescent wave amplification in the visible regime[35,36] and going far beyond the near-field diffraction limit, our method possesses the potential to open a new avenue for nanolithography and superfocusing system.

Principles and results

Figure 1 schematically illustrates the REI enabled by the ring-disk complementary structure. In an ultrathin silver film with thickness *t*, periodical arrayed ring apertures with slit width *w* are etched from the surface down to the silicon dioxide substrate. At the center of each building block, a hole with radius *r* is perforated and a silver nanoring is presented. The dielectric function of silver is obtained from the data measured by Johnson and Christy[37] and the refractive index of silicon dioxide is reckoned as 1.5 for simplicity. A finite difference time domain (FDTD) based solver CST 2014 is adopted to analyze the building block while periodic conditions are used along *x* and *y* directions. The unit cell was meshed with little square elements and local mesh refinement has been ensured ultrafine around the metal and slit regions. This pattern has been chosen because it offers a flexible platform to hybridize the electromagnetic excited surface charges at the inner and outer interfaces due to the finite width of the silver nanoring wall. The inset in fig. 1 describes the top view of the building block, *p* and *g* indicate the lateral width of the building block and the width of the nanoring wall. *w* is the width of the ring aperture surrounding the silver nanoring.

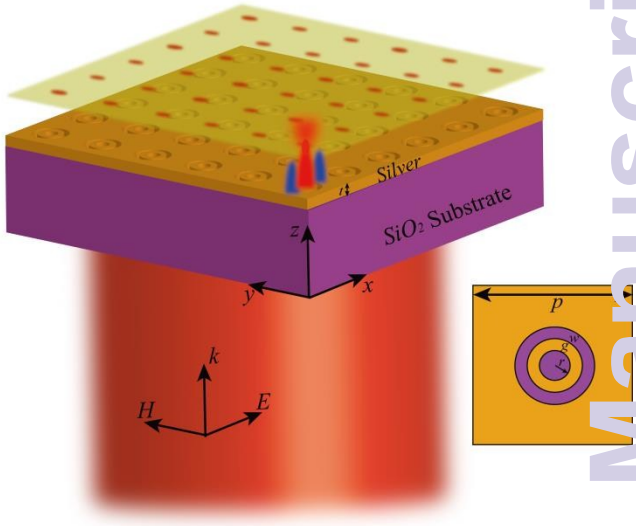

Fig1. An illustration of REI enabled by the ring-disk complementary structure. The red region indicates the *x*-polarized plane wave at wavelength of 633 nm. Abrupt π phase change in one unit cell structure has been schematically shown. The yellow transparent part represents the focal plane decorated with periodically arrayed spots. The inset is the top view of the building block.

Fano resonance

For the case of the nanoring, its plasmon hybridization originated from mixing dipolar bonding resonances of a nanodisk and that of a nanohole is an interesting phenomenon (see in ESI, Fig. S1†).[38,39] These plasmon modes are substantially electromagnetic excitations induced surface charges concentrated at the interfaces between the silver and surrounding medium. The strength of the interaction between the inner and outer surfaces of the nanoring wall is manipulated by the width *g*. This coupling splits the energy distribution into a symmetric bonding mode and an asymmetric anti-bonding mode. Figure S2† in the ESI illustrates how the electromagnetic excited charges distributed at the cross-section *x*-*z* plane of a nanoring when the bonding resonance and anti-bonding resonance occur.

It is noted that the profile of the transmission/absorption spectrum in fig. S2†(b) belongs to the type of Lorentz curve which was recognized as the fundamental lineshape of resonance until Ugo Fano found a new kind of resonance exhibiting an asymmetric lineshape with the following functional form[40]:

$$I = C_1 \frac{(F\gamma + \omega - \omega_0)^2}{(\omega - \omega_0)^2 + \gamma^2} + C_2 \qquad (1)$$

Where C_1 and C_2 are constants, *F* indicates the ratio between resonant and direct scattering probability which describes the degree of asymmetry, ω_0 decides the position of the resonance and γ represents the damping coefficient.

A Fano resonance occurs in the presence of interference between a spectrally broad and narrow mode. In this periodical ring-disk complementary structure, the broadband mode can be supported by the continuum of propagating waves through the silver film since the film is thin enough to be penetrated. The narrowband mode lies in the complex hybrid plasmon mode excited when the ring-disk complementary component integrated at the center of the silver film. This mode can be understood as an interaction of the symmetric bonding mode and the individual plasmon mode of a nanohole.[38,39] In order to make it clear, the transmission line shape of only periodical silver nanorings, the continuing silver film and the ring-disk complementary structure are given as figure 2(a) shows.

As described by the blue dashed curve, an obvious dip exists in the spectrally broad transmission curve, which indicates that a narrowband resonance occurs at about 633 nm. Combined with the analytical data in the fig S2† in the ESI, it is clear that the resonance mode is the symmetric bonding mode. The black dot curve indicates that the transmission line shape of the continuing silver film is rather flat. However, the flat profile will transform into an asymmetric one (red solid curve) when the silver nanoring is integrated in the center, illustrating that a complex hybrid plasmon mode interfering with the continuing propagating waves lead to a plasmonic Fano resonance, which is always induced by a bright broadband mode spectrally overlaps a dark plasmon mode.[25,30]

Figure 2(b) shows a fit of the FR profile to the transmission of the ring-disk complementary structure. When suitably evaluated the four parameters with C_1 = 0.089, C_2 = 0.38, F = 0.97 and γ = 3.6, the analytical mode agrees very well with the FDTD simulation results. From the fit, approximately unity of F means the resonant frequency is located nearly at the half distance between the top and dip of the spectrum, which illustrated that the transmission lineshape possesses the standard FR profile. In addition, the absorption peak at the wavelength near the FR dip (633 nm) shown as the green solid curve confirms that the dark mode has been excited.

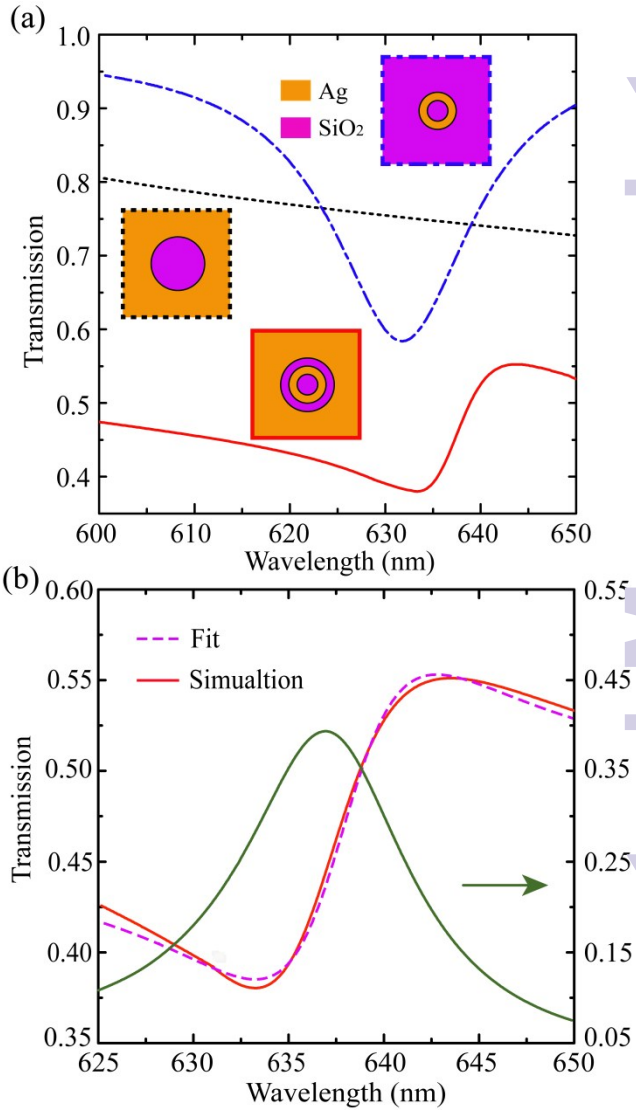

Fig.2 (a) Transmission of the only periodical silver nanorings (blue dashed curve), the continuing silver film (black dot curve) and the ring-disk complementary structure (red solid curve). The three insets are the top view of respective building block as the edge indicates. (b) Zoom-in-plot of the transmission lineshape of the ring disk complementary structure, the purple dashed curve indicates the classical FR formula fitting to the simulated transmission spectrum (red), the green solid curve shows the absorption of the structure from the FDTD simulation.

REI via plasmonic Fano resonance

The Fano resonance provides a platform for the researching of light-matter interaction on the nanoparticles. In the following we show that the field distribution induced by the plasmonic Fano resonance is an ideal candidate to achieve REI and subdiffraction light focusing. Figure 3(a) depicts the electromagnetic fields profiles of the ring-disk complementary structure when plasmonic Fano resonance occurs. The energy distribution shows a remarkable field enhancement at the outer interface of the nanoring wall and in the central nanohole, but diminishes in the silver. Obviously, there is a π-phase jump occurs at the adjacent air channels (the hole and the ring aperture), creating a transverse oscillation in the near field that suppresses radiation and make the evanescent waves interfere destructively in the propagating direction.[12]

The example discussed in this paper is assumed to focus at a distance of 36 nm for a spot as small as 30 nm (FWHM in polarized

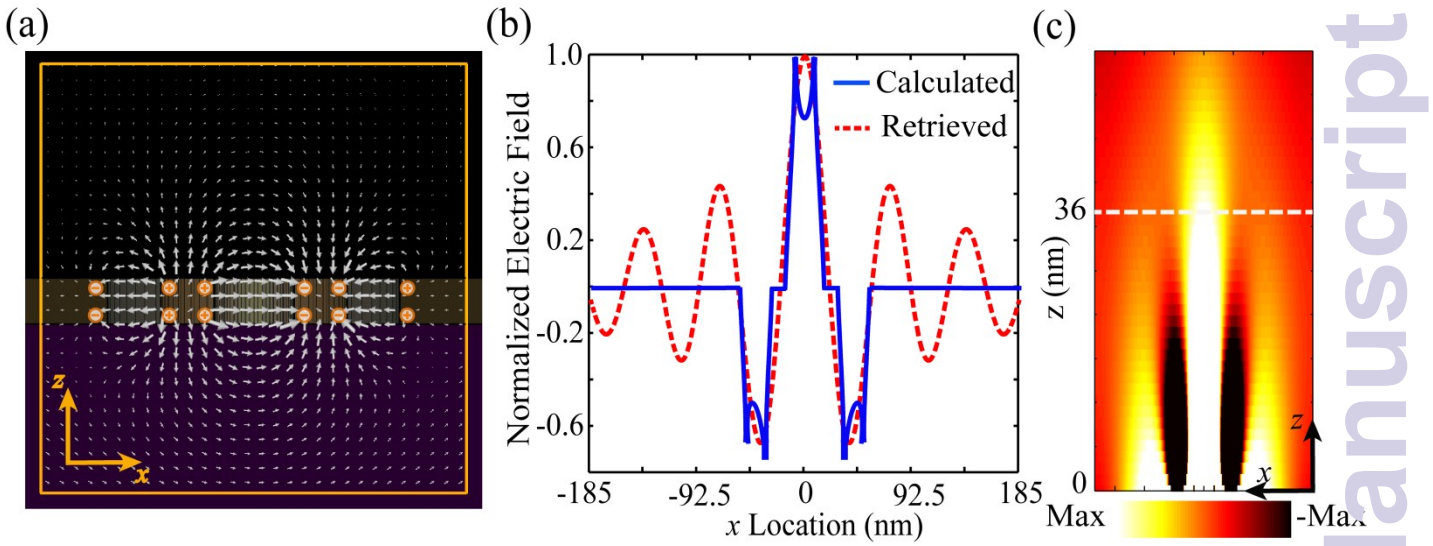

Fig. 3. (a) The field distribution to cross section along *x*-*z* plane for the building block. The orange solid line denotes the region we investigate, the scale and direction of the white arrows indicate the amplitude and direction of the electric field, respectively. The dark yellow part represents silver and the purple part denotes the silicon dioxide. (b) Source distribution back propagated with *x*-polarized FWHM of 28 nm at 36 nm away from the structure (red dashed curve) agrees well with the electric field amplitude envelope exiting the structure (blue solid curve). (c) The REI subdiffraction focusing effect in *x*-*z* plane, the white dashed line indicates the position we investigated.

direction). Figure 3(b) describes the field distribution exiting the structure after propagating backward by 36 nm (red dashed curve) which is calculated by following form:[16]

$$E(x, z=0) = \frac{l\left[l\cos\left(\frac{\pi x}{d}\right) + x\sin\left(\frac{\pi x}{d}\right)\right]}{\left(l^2 + x^2\right)} \quad (2)$$

where x is the distance from the symmetric axis in each building block, l and d represent the focal length and spot size, respectively. Since the field intensity retrieved by (2) is diminished at the outer region by several orders of amount of that in center, thus only three lobes have been discussed here for simplicity. In order to create a rapid transverse oscillation to suppress radiation and generate a narrow central lobe, the width of the nanoring wall g and surrounding ring aperture w should be the same as the interval of the 0-π phase jump. Furthermore, the amplitude envelope that is required in the near field is mainly affected by the size of the silver nanoring and the thickness of the silver film t. Accounting for all these factors, the optimized dimensions are: t = 17 nm, p = 370 nm, d = 30 nm, w = 20 nm and g = 20 nm. The blue solid curve in fig. 3(b) shows the $|E_x|^2$ distribution generated by plasmonic Fano resonance in such structure which is most similar to that depicted by red dashed curve, demonstrating that this ring-disk complementary structure can act as a NFP to modulate both amplitude and phase to produce deep subwavelength focus spots. The electric field alternates sign between adjacent peaks means a π phase shift existing with respect to the neighbour. The REI subdiffraction focusing effect can be clearly seen in fig. 3(c).

Discussion

It should be remembered that the amount of evanescent wave amplification can be measured as l/d,[36] where l is the working distance and d represents the spot size. That is an intuitive picture to show that it is more difficult to obtain a longer focal length for a smaller spot size. In other words, the exponential decay of the evanescent wave limits the working distance. The near-field diffraction limit could be validated by considering that the field emanating from the structure fades to *1/e* of its original value with a characteristic length L.[10,41]

$$L = \frac{1}{4\pi}\frac{1}{\sqrt{\delta^{-2} - \varepsilon\lambda_0^{-2}}} \quad (3)$$

where λ_0 and ε are the wavelength of light in vacuum and the permittivity of air, respectively. In the reference [10], δ indicates the period of the line-array object, corresponding to a characteristic wave vector k_g. However, in the subwavelength focusing system, size of the spot relies on the highest-order of wave vector contributing to the focus. δ in this formula can be understood as the null-to-null beam width of the focal spot.

Figure 4 investigates the metric of evanescent wave amplification in our design. The red points denote the calculated spot sizes corresponding to different focal lengths which have been fitted by the blue solid line. It is intuitive to evaluate the performance of evanescent wave amplification by considering the gradient of the line. Fortunately, the result is ~1.2, indicating that the amount of evanescent wave amplification is double of the results obtained in poor man's perfect lens (0.5 in the UV) and three deeply subwacelength slits system (0.6 in the visible regime).[35] The three insets show the energy distribution corresponding to the planes at 25 nm, 36 nm and 45 nm. The performance of deep subwavelength spot (~30 nm) with almost no background field at z = 36 nm goes far beyond the

near-field diffraction limit, which implied that the largest distance for a spot with FWHM of 30 nm is about 4.7 nm.

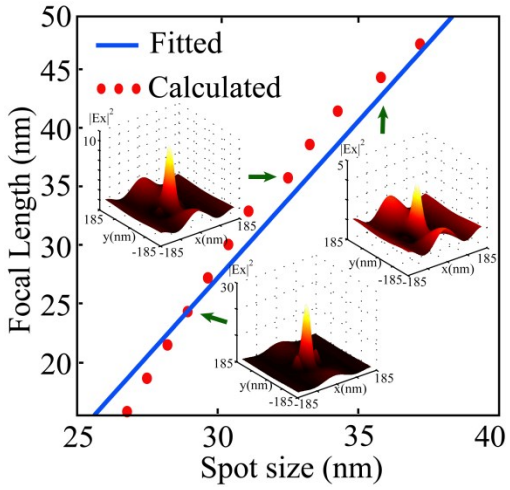

Fig. 4. The relation between the focal length and its corresponding spot size. Calculated results have been described as the discrete red points and fitted by the blue solid line. The three insets detailedly describe the energy distribution at planes of 25 nm, 36 nm and 45 nm as green arrows indicate.

In order to investigate the intensity enhancement at the focal plane which is not typical in REI method and illustrate that the subdiffraction focusing is induced by the destructive interference rather than simple diffraction from the central hole or surrounding slit, different schemes have been compared as shown in the figs 5(a)-(c). The figure 5(a) depicts the design with the optimized coupling. In this case, the energy created by hybrid plasmon resonances at 633 nm is strong enough to boost the field because of the narrow width of the nanoring wall (20 nm). A second contributor to the field enhancement is the plasmonic Fano resonance originated from the interference between the complex hybrid plasmon resonances and the continuum of propagating waves through the silver film. In figure 5(b), one building block with only a central hole is shown. "Subwavelength spot" generated by this sample is based on only near-field diffraction from the hole. Figure 5(c) describes the ring-disk complementary structure with a weaker plasmon coupling between the inner and outer interface of the nanoring wall. Since the distance between the hole and surrounding slit is large, the inner and outer plasmon resonances tend to detune from each other in energy and lead to the dimmer and wider central lobe than that in fig. 5(a), which has been illustrated by the subdiffraction focusing effect (*x*-*y* plane) at 36 nm above the silver film as shown in figs 5(d)-(f). Under the optimized hybrid resonances, the enhancement factor of the light intensity at this plane reaches up to 1.8, nearly 2.2 times larger than that of case *c*. Figure 5(e) indicates that there is almost no field at this distance let alone focusing, which is in accordance with the near-field diffraction limit. The intensity distribution of focus in fig. 5(d) is shown as red solid curves in figs 5(g)-(h). The FWHM for *x* (FWHM*x*) and *y* (FWHM*y*) polarizations are 31 nm and 58 nm, respectively, which indicate that the energy converges into a spot as small as $0.0045\lambda^2$, indeed a deep subwavelength size. The less ideal focusing is caused by the imperfect reproduction of the retrieved source field distribution and the sharply peaked field at the silver-air interfaces. Perhaps, engaging multi[ple] surrounding slits instead of a single one as a plasmo[nic] hybridization generator is an effective method to optimize th[e] focal spot since the more complicated coupling may lead to [a] perfect reproduction of the retrieved field distribution. Fo[r] comparison, field distribution in figs 5(e)-(f) are displayed by the blue and black dashed curves. The FWHM*x* and FWHM*y* fo[r] the weakly coupled ring-disk complementary structure are 88 nm and 172 nm, respectively, leading to a spot size of 0.0378λ^2, about 8 times larger than that produced by the optimized design.

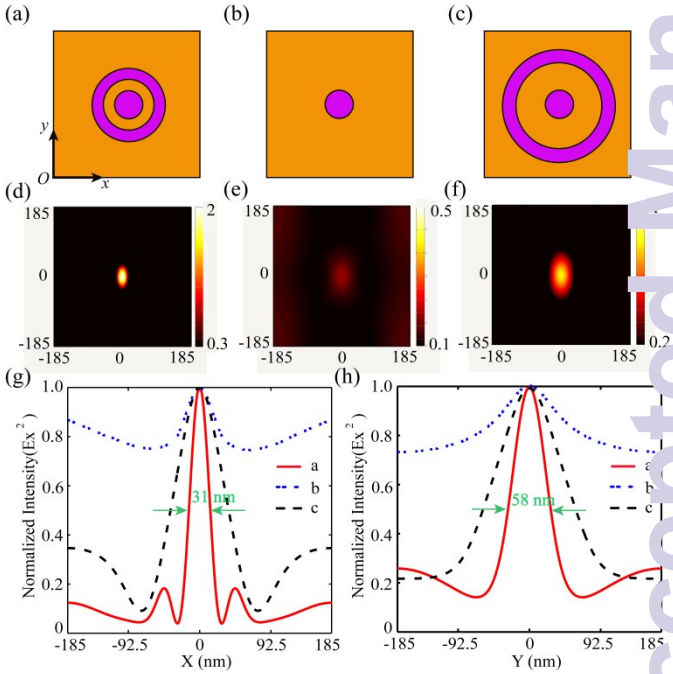

Fig.5 (a)-(c) Different schemes for comparison. (a) The optimized building block with the dimensions proposed before. (b) The building block with only a hole. (c) The w[ell] coupled ring-disk complementary structure. (d)-(f) The subdiffraction focusing effect (*x*-*y* plane) at 36 nm above the silver film corresponding to (a)-(c). (g)-(h) The *x* component of electric fields intensity distribution at 36 nm above the silver film along the (g) *x* direction and (h) *y* direction. Red solid curves represent the performance [of] the case in (d). The blue and black dashed curves stand for the performances of the case in (e) and (f).

This ring-disk complementary structure can be viewed a[s] coupled antennas and the excitation of REI relies on two mechanisms. First, the nanoring converts part of the incident energy to a hybrid plasmon mode (a bonding resonance) by launching SPs and mixing double dipolar resonances. Second, the nanoring couples with the silver film and excite[s] a plasmonic Fano resonance. The coupling offers the platform t[o] create the transverse oscillation that modulates phase and amplitude profile to produce REI subdiffraction focusing. The achieved intensity enhancement factor is affected by the finite number of unit cells. Figure S3† shows the dependencies [of] the intensity enhancement on the total numbers of building blocks *N*. The calculated data indicates that the maximal electric field at the focal plane (*l* = 36 nm) with 25 unit c[ells]

and 81 unit cells are 1.1 and 1.6 times larger than the incident field, respectively. However, the enhancement saturated when *N* reaches 225, indicating that this spectral collapse effect is not so strong as that existed in the coherent metamaterial.[42,43] It can be concluded that the periodicity requirement will not restrict the ring-disk complementary structure's potential applications since limited numbers of building blocks can obtain ideal intensity enhancement.

This work is reminiscent of, but the physics inside is different from the REI methods proposed before.[17,35] A metal-dielectric waveguide array possesses ability to realize rapid fields oscillation for subdiffraction focusing when the highest-order mode is excited.[17] However, this ring-disk complementary structure can function as a NFP by directly linearly polarized plane wave excitation. Fano resonance of multiple slits system can also achieve subdiffraction focusing,[35] where destructive interference is the physical connection to REI. Different from the interference between the propagating modes excited in the slits, localized complex hybrid plasmon mode interferes with the continuum of propagating waves realizing prescribed phase intervals and amplitude profiles at the immediate proximity of the structure. In addition, our design relaxes the requirement of ultra thick metal slab utilized in references [17] and [35]. At optical regimes, the skin depth of metal is almost comparative to the sampling interval required for REI,[17] which leads to a strong near-field diffractive coupling and restricts the focusing quality. Interestingly, our design takes advantage of this intimate coupling, where plasmonic Fano resonance excited to realize abrupt π phase change and amplitude modulation within small fraction of a wavelength.

Conclusions

In summary, this paper suggests a ring-disk complementary design to achieve subdiffraction focusing combined with evanescent wave amplification. Abrupt π phase change, amplitude modulation and intensity enhancement of the focal spot are contributed by the plasmonic Fano resonance. With benefits of modes coupling, the far-field incident energy can converge into a deep subwavelength spot as small as $0.0045\lambda^2$ and the focal intensity gets enhancement up to 1.8 times compared to the incident field at 36 nm above the silver film, which goes far beyond the near-field diffraction limit and exceeds the metric of evanescent wave amplification. This is of interest to a myriad of applications such as near-field imaging and spectroscopy which need a probe that operates at a distance. We believe the plasmonic Fano resonance will be an effective method for the design of the subdiffraction focusing systems.

Acknowledgements

This work was supported by the 973 Program of China (no. 2013CBA01700) and the National Natural Science Funds (no. 61138002).

Notes and references

1 E. Abbe, *Archiv Mikr. Anat.*, 1873, 9, 413-420.
2 E. T. F. Rogers, J. Lindberg, T. Roy, S. Savo, J. E. Chad, M. R. Dennis, and N. I. Zheludev, *Nat. Mater.*, 2012, 11, 432-435.
3 D. Tang, C. Wang, Z. Zhao, Y. Wang, M. Pu, X. Li, P. Gao, and X. Luo, *Laser & Photon. Rev.*, 2015, 1-7.
4 M. Pu, X. Li, X. Ma, Y. Wang, Z. Zhao, C. Wang, C. Hu, P. Gao, C. Huang, H. Ren, X. Li, F. Qin, M. Gu, M. Hong, and X. Luo, *Sci. Adv.*, 2015, 1, e1500396.
5 D. K. Gramotnev, and S. I. Bozhevolnyi, *Nat. photonics*, 2014, 8, 13-22.
6 M. Xiao, *Opt. Commun.*, 1996, 132, 403-409.
7 J. B. Pendry, *Phys. Rev. Lett.*, 2000, 85, 3966-3969.
8 A. Grbic, and G. V. Eleftheriades, *Phys. Rev. Lett.,* 2004, 92, 117403.
9 T. Taubner, D. Korobkin, Y. Urzhumov, G. Shvets, R. Hillenbrand, *Science*, 2006, 313, 1595.
10 N. Fang, H. Lee, C. Sun, and X. Zhang, *Science*, 2005, 308, 534-537.
11 J. Valentine, S. Zhang, T. Zentgraf, E. Ulin-Avila, D. A. Genov, G. Bartal, X. Zhang, *Nature*, 2008, 455, 376.
12 R. Merlin, *Science*, 2007, 317, 927-929.
13 F. M. Imani, and A. Grbic, *IEEE Trans. Antennas Propag.*, 2012, 60, 3155-3164.
14 X. Luo, M. Pu, X. Ma, and X. Li, *Inter. J. Antenn. Propag*. 2015, 2015, 204127.
15 A. Grbic, and R. Merlin, *IEEE Trans. Antennas Propag.,* 2008, 56, 3159-3165.
16 A. Grbic, L. Jiang, and R. Merlin, *Science*, 2008, 320, 511-513.
17 R. Gordon, *Phys. Rev. Lett.*, 2009, 102, 207402.
18 Y. Wang, A. M. Wong, L. Markley, A. S. Helmy, and G. V. Eleftheriades, *Opt. Express*. 2009, 17, 12351-12361.
19 V. Intaraprasonk, Z. Yu, and S. Fan, *Opt. Lett.*, 2010, 35, 1659-1661.
20 L. Li, F. Li, T. Cui, and K. Yao, *Opt. Express*, 2015, 23, 401-412.
21 X. Luo and T. Ishihara, *Appl. Phys. Lett*., 2004, 84, 4780–4782.
22 X. Luo and L. Yan, *IEEE Photonics J.*, 2012, 4, 590–595.
23 J. Luo, B. Zeng, C. Wang, P. Gao, K. Liu, M. Pu, J. Jin, Z. Zhao, X. Li, H. Yu, and X. Luo, *Nanoscale*, 2015, DOI: 10.1039/C5NR05153C
24 M. Pu, M. Song, H. Yu, C. Hu, M. Wang, X. Wu, J. Luo, Z. Zhang, and X. Luo, *Appl. Phys. Express*, 2014, 7, 032002.
25 M. Rahmani, B. Lukiyanchuk, and M. Hong, *Laser & Photon. Rev.*, 2013, 7, 329-349.
26 Z. Yang, Z. Hao, H. Lin, and Q. Wang, *Nanoscale*, 2014, 6, 4985-4997.
27 B. Zeng, Y. Gao, and F. J. Bartoli, *Appl. Phys. Lett.*, 2014, 105, 161106.
28 B. Zeng, Y. Gao, and F. J. Bartoli, *Sci. Rep*., 2013, 3, 2840.
29 Z. Liao, B. Pan, X. Shen, and T. Cui, *Opt. Express*, 2014, 22, 15710-15717.
30 M. Rahmani, D. Lei, V. Giannini, B. Lukiyanchuk, M. Ranjbar, T. Y. F. Liew, M. Hong, and S. A. Maier, *Nano Lett.*, 2012, 12, 2101-2106.
31 X. Wei, M. Altissimo, T. J. Davis, and P. Mulvaney, *Nanoscale*, 2014, 6, 5372-5377.
32 Y. Zhang, T. Li, B. Zeng, H. Zhang, H. Lv, X. Huang, W. Zhang, and A. K. Azad, *Nanoscale*, 2015, 7, 12682-12688.
33 M. Amin, M. Farhat, and H. Bagci, *Sci. Rep*., 2013, 3, 2105.
34 M. Song, H. Yu, C. Wang, N. Yao, M. Pu, J. Luo, Z. Zhang, and X. Luo, *Opt. Express*, 2015, 23, 2895-2903.
35 S. Chen, S. Jin, and R. Gordon, *Phys. Rev. X*, 2014, 4, 031021.
36 R. Gordon, *Opt. Lett*., 2012, 37, 912-914.
37 P. B. Johnson, and R. W. Christy, *Phys. Rev. B*, 1972, 6, 4370-4379.
38 E. Prodan, C. Radloff, N. J. Halas, and P. Nordlander, *Science*, 2003, 302, 419-422.

39 P. Nordlander, *ACS Nano*, 2009, 3, 488-492.
40 B. Lukyanchuk, N. I. Zheludev, S. A. Maier, N. J. Halas, P. Nordlander, H. Giessen, and C. T. Chong, *Nat. Mater.,* 2010, 9, 707-715.
41 Z. Zhao, Y. Luo, W. Zhang, C. Wang, P. Gao, Y. Wang, M. Pu, N. Yao, C. Zhao, and X. Luo, *Sci. Rep*., 2015, 5, 15320-15330.
42 V. A. Fedotov, N. Papasimakis, E. Plum, A. Bitzer, M. Walther, P. Kuo, D. P. Tsai, and N. I. Zheludev, *Phys. Rev. Lett.*, 2010, 104, 223901.
43 M. Pu, C. Hu, C. Huang, C. Wang, Z. Zhao, Y. Wang, and X. Luo, *Opt. Express*, 2013, 21, 992-1001.